



Obliquity variations of a moonless Earth

Jack J. Lissauer^a, Jason W. Barnes^{a,b,*}, John E. Chambers^c

^aNASA Ames Research Center, Space Science and Astrobiology Division, M/S 245-3, Moffett Field, CA 94035, United States

^bUniversity of Idaho, Department of Physics, Campus Box 440903, Moscow, ID 83844-0903, United States

^cDepartment of Terrestrial Magnetism, Carnegie Institution for Science, 5241 Broad Branch Rd., NW, Washington, DC 20015, United States

ARTICLE INFO

Article history:

Received 22 December 2010

Revised 6 August 2011

Accepted 18 October 2011

Available online 28 October 2011

Keywords:

Astrobiology

Earth

Extrasolar planets

Rotational dynamics

ABSTRACT

We numerically explore the obliquity (axial tilt) variations of a hypothetical moonless Earth. Previous work has shown that the Earth's Moon stabilizes Earth's obliquity such that it remains within a narrow range, between 22.1° and 24.5°. Without lunar influence, a frequency map analysis by Laskar et al. (Laskar, J., Joutel, F., Robutel, P. [1993]. *Nature* 361, 615–617) showed that the obliquity could vary between 0° and 85°. This has left an impression in the astrobiology community that a big moon is necessary to maintain a habitable climate on an Earth-like planet. Using a modified version of the orbital integrator *mercury*, we calculate the obliquity evolution for moonless Earths with various initial conditions for up to 4 Gyr. We find that while obliquity varies significantly more than that of the actual Earth over 100,000 year timescales, the obliquity remains within a constrained range, typically 20–25° in extent, for timescales of hundreds of millions of years. None of our Solar System integrations in which planetary orbits behave in a typical manner show obliquity accessing more than 65% of the full range allowed by frequency-map analysis. The obliquities of moonless Earths that rotate in the retrograde direction are more stable than those of prograde rotators. The total obliquity range explored for moonless Earths with rotation periods less than 12 h is much less than that for slower-rotating moonless Earths. A large moon thus does not seem to be needed to stabilize the obliquity of an Earth-like planet on timescales relevant to the development of advanced life.

© 2011 Elsevier Inc. All rights reserved.

1. Introduction

Inhabitants of Earth enjoy a relatively benign and stable climate in part because our planet's obliquity, Ψ , which is the angle between its orbital angular momentum and its rotational angular momentum, does not vary by a large amount. In contrast, the obliquity of Mars ranges from $\sim 0^\circ$ to 60° (Laskar et al., 1993b, 2004). The value of Ψ is an important factor in determining climate and habitability. For $\Psi < 54^\circ$ or $\Psi > 126^\circ$, a planet on a low-eccentricity orbit receives more radiant energy from its star (averaged over time) at equatorial latitudes than near its poles, while the poles are heated most for obliquities $54^\circ < \Psi < 126^\circ$. In contrast, the poles receive very little light for Ψ near 0° or near 180° (Fig. 1). (See Dobrovolskis (2009) for a discussion of the illumination of high-obliquity planets.)

Theoretical analyses have not yet determined whether terrestrial planets are formed with a preference for low Ψ , as Earth and Mars have at the present epoch (Schlichting and Sari, 2007), or whether the rotation axes of rocky bodies are essentially ran-

domly distributed (Lissauer et al., 1997, 2000). Recent numerical studies suggest that distribution of orientations of initial rotation axes may well be isotropic (Miguel and Brunini, 2010). Stellar tides affect the obliquity evolution of close-in planets like Mercury and Venus – these effects are beyond the scope of our present work.

Torques from the pull of other planets on the equatorial bulge of a planet can alter its axial tilt. Therefore, Ψ does not necessarily remain fixed subsequent to the epoch of planetary accretion. Laskar and Robutel (1993) analyzed possible obliquity variations of the planets in our Solar System. Their study also considered the same planets with different rotation periods, and the Earth without the Moon. Using frequency map analysis, they found that the obliquity of Mars can range from 0° to 60° , and a hypothetical moonless Earth's axial tilt could be close to 0° or as large as 85° (Laskar and Robutel, 1993; Laskar et al., 1993b). In contrast, Ψ of the actual Earth varies far less, from 22° to 24.6° , because of the Moon's stabilizing influence (e.g., Laskar et al., 1993a,b). Numerical integrations (Laskar et al., 2004) have shown that Mars's obliquity varies over most of its permitted range on timescales of tens of millions of years. Neron de Surgy and Laskar (1997) show that tidal evolution of the Earth–Moon system is expected to drive the Earth's rotation into the chaotic zone within 1.5–4.5 Gyr, leading to the likelihood of excursions of Earth's obliquity to values above 80° at some point within the next ~ 6 Gyr.

* Corresponding author at: University of Idaho, Department of Physics, Campus Box 440903, Moscow, ID 83844-0903, United States.

E-mail addresses: jack.j.lissauer@nasa.gov (J.J. Lissauer), jwbarnes@uidaho.edu (J.W. Barnes).

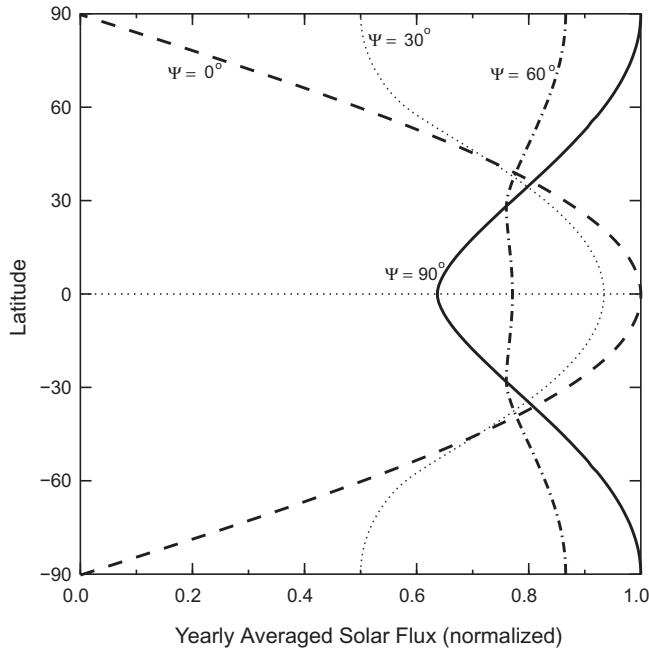


Fig. 1. Yearly averaged solar flux (normalized) for a hypothetical planet with varying obliquities of 0° (dashed line), 30° (dotted line), 60° (dot-dashed line), and 90° (solid line). The greatest flux disparity occurs at $\Psi = 0^\circ$; the most nearly even flux distribution occurs near $\Psi = 54^\circ$. Note, however, that seasonal variations in diurnally averaged solar flux are larger for higher obliquity.

It has been asserted that the presence of a large moon may be required for Earth (Laskar et al., 1993b), or indeed any terrestrial planet (Ward and Brownlee, 2000) to have a stable enough obliquity and benign enough climate for advanced life to develop, and astrobiology textbooks often state that climate stability for moonless earthlike planets with rotation periods comparable to 24 h have wild swings in obliquity (Goldsmith and Owen, 2002; Lunine, 2005). If a large moon is indeed needed to make a planet a viable abode, then the number of habitable planets in our galaxy capable of nurturing advanced life is likely to be one or two orders of magnitude lower than if no such requirement exists.

We thus study herein the long-term obliquity evolution of a moonless Earth with constant rotation rate numerically using a variant of the symplectic orbital integrator `mercury` programmed to implement the algorithm of Touma and Wisdom (1994). We describe this algorithm and the parameters that we use in Section 2. Section 3 describes the ± 2 Gyr integration of a “standard” moonless Earth (“Earthmoo”). We study chaotic effects using integrations with slightly different initial conditions in Section 4. We also investigate substantively differing sets of initial conditions, including varying the initial rotational axis azimuth (Section 5), obliquity (Section 6), and planetary rotation rate (Section 7). Concluding remarks are presented in the final section.

2. Methods

2.1. Spin-tracking

The evolution of Earthmoo’s obliquity is calculated using a modified version of the mixed-variable symplectic (MVS) integrator that we have incorporated into the `mercury` package developed by Chambers (1999). The MVS algorithm is a descendant of the symplectic mapping of Wisdom and Holman (1991). The Earth is treated as an axisymmetric rigid body, and its orbital and rotational evolution is calculated, subject to gravitational interactions

with the Sun and planets, following the procedure described in detail by Touma and Wisdom (1994).

The Hamiltonian for a system of N planets orbiting a star can be written as

$$H = H_{\text{kepler}} + H_{\text{int}} + H_{\text{jump}} + H_{\text{euler}}, \quad (1)$$

where

$$H_{\text{kepler}} = \sum_{i=1}^N \left(\frac{p_i^2}{2m_i} - \frac{Gm_0m_i}{r_{i0}} \right),$$

$$H_{\text{int}} = - \sum_{i=1}^N \sum_{j>i}^N \frac{Gm_im_j}{r_{ij}} - \sum_{i \neq 1} \left(\frac{Gm_i}{2R_{i1}^3} \text{tr}(I) - \frac{3}{2} \frac{Gm_i}{R_{i1}^5} \mathbf{R}_{i1} \cdot \mathbf{I} \mathbf{R}_{i1} \right), \quad (2)$$

$$H_{\text{jump}} = \frac{1}{2m_0} \left(\sum_{i=1}^N \mathbf{p}_i \right)^2,$$

$$H_{\text{euler}} = \frac{1}{2} \mathbf{S} \cdot \mathbf{I}^{-1} \mathbf{S}.$$

In Eq. (2), m_i is the mass of planet i , and m_0 is the mass of the star. The position, momentum, and spin angular momentum vectors in an inertial frame centered on the center of mass of the system are denoted by \mathbf{r} , \mathbf{p} , and \mathbf{s} , respectively. \mathbf{R} , \mathbf{P} , and \mathbf{S} are the equivalent vectors measured in a frame rotating with the rigid body, measured from its center of mass. Here, I is the inertia tensor for the rigid body, and $\text{tr}(I)$ indicates the trace of I , where $\text{tr}(I) \equiv \sum_{k=1, \dots, 3} I_{kk}$. Note that the star has index 0 in the above expressions, while the rigid body has index 1. Following Touma and Wisdom (1994), we retain only low-order terms in the expansion for the gravitational interaction between the rigid body and the other bodies in the system, which are themselves assumed to be point masses.

Following the usual practice for symplectic integrators, the system is advanced under each part of H separately, in this case following a leapfrog scheme:

- Advance H_{int} for $\tau/2$.
- Advance H_{jump} for $\tau/2$.
- Advance H_{kepler} and H_{euler} for τ .
- Advance H_{jump} for $\tau/2$.
- Advance H_{int} for $\tau/2$.

This algorithm is accurate to second order in the timestep τ . The Hamiltonian pieces H_{kepler} and H_{euler} affect separate sets of variables, so they can be advanced in parallel.

We set up the rigid body frame so that its axes are aligned with the principal axes of the body, in which case I is diagonalized, with diagonal elements I_1 , I_2 and I_3 , where $I_1 = I_2$ for an axisymmetric body. The system can be advanced under H_{euler} using Euler’s equations, which in this case have the solution

$$\begin{aligned} S_1(t) &= S_1(0) \cos(\alpha t) + S_2(0) \sin(\alpha t), \\ S_2(t) &= -S_1(0) \sin(\alpha t) + S_2(0) \cos(\alpha t), \\ S_3(t) &= S_3(0), \end{aligned} \quad (3)$$

where (for axisymmetric bodies such as Earth)

$$\alpha = \left(\frac{1}{I_3} - \frac{1}{I_1} \right) S_3(0). \quad (4)$$

Each time H_{euler} is advanced, it is also necessary to update the matrix that transforms between the two reference frames. This is done using the procedure described by Touma and Wisdom (1994).

The interaction Hamiltonian H_{int} can be advanced by noting that it depends only on the position coordinates, so these remain fixed while the momenta undergo an impulse. Similarly, under H_{jump} , the momenta are fixed while the positions change. The Keplerian orbits of the planets are advanced under H_{kepler} using Gauss’s f and g functions (see Danby, 1988), noting that \mathbf{r}_{i0} and \mathbf{p}_i are

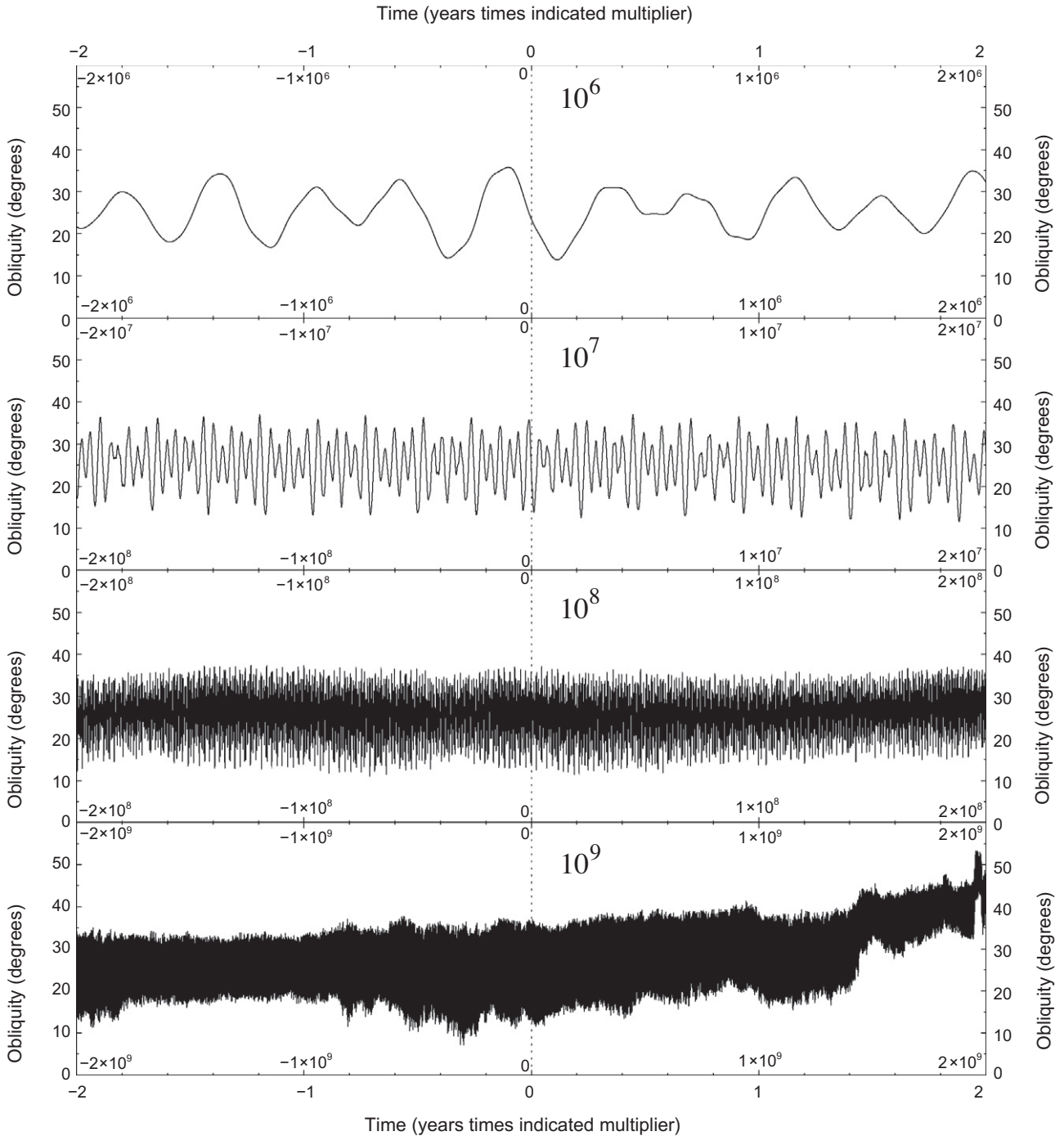


Fig. 2. Firstrun Earthmoo’s obliquity through time is displayed at four different timescales: millions of years (top), tens of millions of years (second from top), hundreds of millions of years (third from top), and billions of years (bottom). The integration extends 2 Gyr forward and backward from the present day. Though obliquity varies significantly more than the real Earth on a timescale of hundreds of thousands of years, the variations remain constrained on tens and hundreds of millions of year timescales. At billion-year timescales the envelope of variation changes.

canonically conjugate. We have verified this code by simulating the evolution of Mars’ obliquity over timescales of millions of years and comparing our results to published integrations.

The resulting spin-tracking algorithm spends the majority of its time (>80%) calculating the orbital evolution of the 8-planet system. To improve the computational duty cycle, we have implemented a system whereby we track the spin evolution of multiple “ghost planets” all during a single orbital integration. We assign the ghost planets appropriately diverse initial obliquities and axis azimuths, but then track their spin evolution as if they

were all in the same spatial location as the “real” Earthmoo at each timestep.

As we have implemented them, the rotational bulges of the planets, excluding the “real” (non-ghost) Earthmoo, do not affect the orbits of the other real planets. The results for ghost planets therefore violate Newton’s third law. However, the neglected accelerations are small, and hence given the inherently chaotic nature of the Solar System planets’ orbits (e.g., Laskar, 1989), the qualitative behavior of the resulting calculation should not differ significantly from one that would track the evolution of both spin and orbits

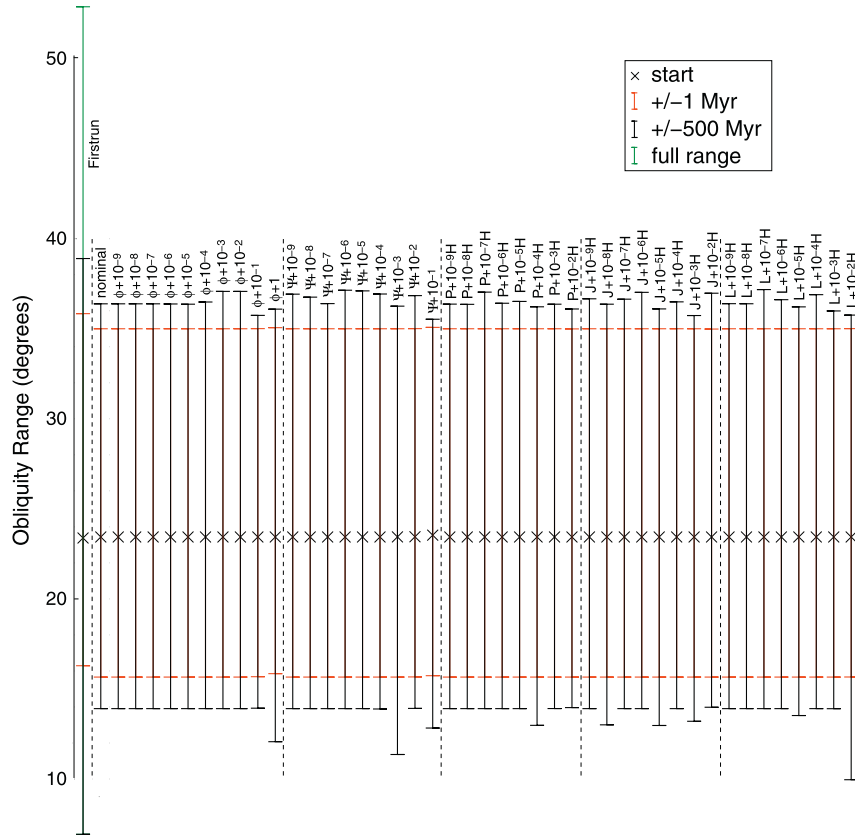


Fig. 3. Here we show the obliquity range for integrations of standard Earthmoons, all with close to Earth’s present J_2 , moment of inertia coefficient, in order to examine the effects of chaos. The range of Firstrun is shown on the left. All other simulations represented had identical planet positions; these positions differed from Firstrun only by the chaotic magnification of small initial differences. While planetary positions are identical, each of these Earthmoons has slightly different starting conditions including different axis azimuths (φ), gravitational moments J_2 (J), moment of inertia (L), rotation period (P), and obliquity (Ψ), as indicated. The red bars show the obliquity sampled during the interval (± 1 Myr). Black bars show the extension of the range of obliquity during the interval (± 500 Myr). Green bars show the obliquity range over the entirety of the relevant integration. The ‘full’ range is ± 2 Gyr for Firstrun and -550 to $+936$ Myr for all other integrations. Note that for all of the integrations shown apart from Firstrun, the full range is identical to the ± 500 Myr range, and the lower obliquity limit for Firstrun is also identical to that in the ± 500 Myr interval. (For interpretation of the references to color in this figure legend, the reader is referred to the web version of this article.)

independently for each case. We also neglect relativistic effects in our calculations. The present version of `mercury` allows us to follow only one planet’s obliquity – Earthmoon for the present work.

2.2. Assumptions and initial conditions

In order to preserve to first approximation interactions with the other Solar System planets, we use a total mass equal to the sum of the masses of the Earth and Moon and give it the initial position and velocity of the center of mass of the Earth–Moon system. We call the resulting object an “Earthmoon” after its designation within the 8-character size limitation for object names within `mercury`. We assume that the density of an Earthmoon would be the same as that of the real Earth, 5.5153 g/cm^3 . The actual density of a planet formed by combining the Earth and the Moon would not differ substantially from this value. The addition of low-density lunar material would lower the body’s density, whereas the resulting compression of the rest of Earth’s volume given the newly greater overburden pressure would raise it. We assume a moment of inertia coefficient C (Ahrens, 1995):

$$C \equiv \frac{C}{M_p R_{eq}^2} = C_{\oplus} = 0.3296108, \quad (5)$$

where C is the planet’s moment of inertia around the principal axis with the greatest moment of inertia, M_p is the mass of the planet (in this case that of Earthmoon), and R_{eq} is the planet’s equatorial radius.

For the nominal Earthmoon case, we use a dynamical oblateness of $J_2 = 0.00108263$ and assume a rotation period of 23 h:56 m:04s.

Because the Solar System is chaotic on timescales of several million years (Laskar, 1989), the results of these very long-term integrations are valid only in a statistical sense. Any one simulation may, indeed, be a statistical fluke, sampling a tiny region of parameter space. Numerous additional simulations of the system must be run in order to obtain a statistically robust distribution of results. To that end, we first explore the obliquity evolution of Earthmoons that differ only slightly from the standard one. In Section 4 we assign initial axis azimuths φ_0 that vary from the standard Earthmoon by 0.1° , 0.01° , 10^{-3° , 10^{-4° , 10^{-5° , 10^{-6° , 10^{-7° , 10^{-8° , and 10^{-9° . The latter few differ by such a minute amount that the difference is actually less than the accuracy of the integration, and thus they diverge more rapidly than they would with perfect accuracy. We employ similar variations over many decades in the changed parameter for initial obliquity Ψ_0 , planetary J_2 , moment of inertia, and rotation period.

Later we look at larger-scale variations of the initial conditions. We investigate a variety of initial obliquities, azimuthal axis orientations, and rotational periods. In Section 5, we vary the initial axis azimuth φ_0 from 0° to 315° in 45° increments. In Section 6, we look at both prograde ($\Psi_0 = 0-90^\circ$ in 15° increments) and retrograde ($\Psi_0 = 135^\circ$, 156° , and 180°) initial obliquities. For varying initial rotation rates in Section 7, we perform runs with sidereal rotation periods of 2.8 h, 4 h, 8 h, 12 h, 14.9590278 and 19.6183971 h (for comparison with Laskar and Robutel (1993)), 16 h, 20 h, 23 h

56 min 4 s, 24 h, 32 h, 40 h, and 48 h. The case of differing rotational periods presents a challenge in that such planets would have values of gravitational moment J_2 and equatorial radius R_{eq} that differ from those of the real Earth. Some of these we explore both prograde and retrograde (*i.e.*, with $\Psi_0 = 156^\circ$ and $\varphi_0 = 180^\circ$) and with Darwin–Radau derived J_2 values (see Appendix A).

3. Standard Earthmoo

Fig. 2 shows the results of the first integration that we performed, that of an Earthmoo with the same spin rate, obliquity, axis azimuth, and J_2 as the real Earth. We refer to this simulation as Firstrun. This was prior to the incorporation of the ghost planets, and its initial obliquity differs slightly from analogous planets in other runs (Fig. 3). We integrated the present Solar System forward and backwards for 2 Gyr and found that, unlike the Martian obliquity, Earthmoo’s obliquity may well *not* explore the majority of the range of values allowed to it by frequency map analysis on time-scales relevant to the evolution of advanced life forms.

The backward integration 2 Gyr into the past is relatively quiet, with obliquity oscillations around an average value of $\sim 25^\circ$ and envelopes varying in width from 13° ($19\text{--}32^\circ$) to 27° ($8\text{--}35^\circ$). The near-future shows similar muted variability. Earthmoo’s average obliquity rises linearly from 25° today to nearly 30° once the integration has simulated 900 Myr into the future. The width of the envelope remains similar, though, at around 18° minimum to maximum. Out as far as 1.4 Gyr into the future, our integration shows Earthmoo’s obliquity quietly confined to values $\lesssim 40^\circ$. Around 1.44 Gyr, the obliquity regime undergoes a shift. The average obliquity increases from 33° to 36° over 5 Myr. At the same time, the obliquity envelope shifts from $25\text{--}42^\circ$ to $29\text{--}44^\circ$. A similar regime shift occurs when the average obliquity spikes up to 48° just prior to 2 Gyr. At that time, the range of the envelope within which the obliquity varies decreases, while the average obliquity increases from 40° to 48° in two stages across 10 Myr. We see obliquity variability regime shifts like these two in some of our other integrations.

4. Chaos

To test the sensitivity of our results to our assigned initial conditions, we integrated a set of ghost Earthmoos simultaneously with the ‘solid’ Earthmoo Firstrun. Each ghost particle started with different initial parameters to the Firstrun Earthmoo above, including one (SQ023A00) with updated (just slightly different) initial obliquity than Firstrun. For these ghost particles, we selected different initial Earthmoo obliquity values Ψ_0 , adding between 10^{-9} and 10^{-10} ; Earthmoos with different axis angles φ_0 , adding $\Delta\varphi = 10^{-9}, \dots, 10^{0}$; Earthmoos with different rotation periods, adding $\Delta P = 10^{-9}, \dots, 10^{-2}$ h (with shape changed to correspond to rotation rate variations as described in Appendix A); Earthmoos with different values for J_2 as would arise from changing Earthmoo’s rotation period by between 10^{-2} and 10^{-9} h (see Appendix A); and Earthmoos with different moments of inertia, L , appropriate for rotation period, p , differing from the nominal value by an amount corresponding to the response of a fluid to changes in the rotation period of Earthmoo by between 10^{-2} and 10^{-9} h. The total obliquity range that each of these Earthmoos explored over the course of their integration is shown in Fig. 3.

We find that over short timescales, (± 1 Myr), these small changes in initial conditions has very little effect on the total obliquity range explored. On ± 500 Myr and longer timescales the range explored starts to diverge, even for nearly equivalent initial conditions. All of the obliquities, however, vary between $\sim 13^\circ$ and $\sim 37^\circ$, and none leaves that range over the course of ± 500 Myr.

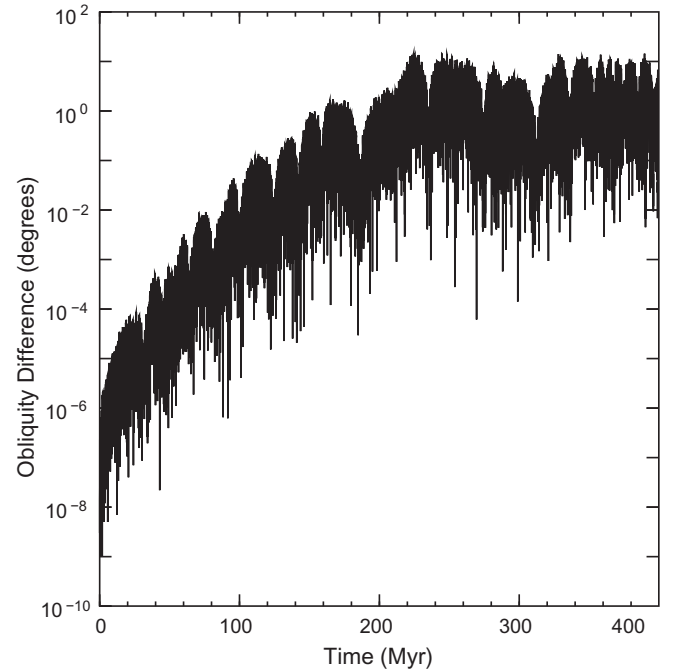


Fig. 4. Plot of the absolute value of the difference between obliquity for two Earthmoos in the same orbital integration (using nominal Solar System parameters) for which the starting axis azimuths φ_0 are 10^{-7} (designated $\phi + 10^{-7}$ in Fig. 3) and 10^{-6} ($\phi + 10^{-6}$ in Fig. 3). As orbital chaos is suppressed, this plot shows only the chaos owing to variations in obliquity. The curve shows a characteristic Lyapunov increase in its upper boundary, but short-term pseudoperiodic variations drive typical differences to be less.

The differences between the solutions discussed above owe to chaos. We test for the influence of chaos in two different ways. We looked for the effects of: (1) pure obliquity chaos, and (2) orbital obliquity chaos.

4.1. Obliquity chaos

In Fig. 4, we show the difference between the obliquity of two different ghost planets with slightly different initial obliquities (differing by 9×10^{-7}). These two ghost planets were in the same orbital integration. Hence the evolution of the obliquity difference between these two ghost planets over time does not result from differences in the positions of the planets.

An exponential increase in the obliquity difference in the two integrations is established at an early stage, and continues until the divergence saturates. Because both obliquities show pseudoperiodic short-term variability, though there are times when the obliquities grow closer by chance. After 240 Myr or so each planet is undergoing pseudoperiodic variations within the same range, and the maximum extent of that range has been reached. After that time, the obliquity difference between the two integrations is stochastically distributed below the maximum range difference. Using the upper envelope of the difference curve, we calculate a Lyapunov time for obliquity chaos of an Earthmoo of 14 Myr – about twice as large as the typical value for the orbits of the terrestrial planets. After roughly 240 Myr, any two ghost planets, even with trivially different initial conditions and everything else equal, can be in fundamentally different obliquity states from one another.

4.2. Orbital chaos

For the orbital chaos test, we ran orbital integrations for identical Earthmoos in Solar Systems with Mars shifted along its orbit by

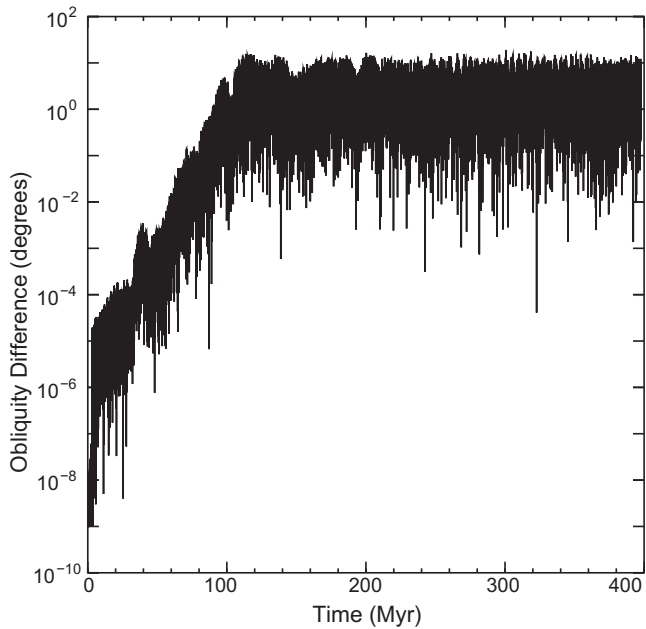


Fig. 5. Plot of the absolute value of the difference between obliquity for two identical Earthmoos in Solar Systems for which Mars' starting location differs by 2 m along its orbit. This diagram shows the more rapid chaotic evolution of Earthmoos obliquities resulting from orbital chaos compared to the obliquity-only chaos displayed in Fig. 4.

1 m in the prograde direction (“ahead”) and by 1 m in the retrograde direction (“behind”). Each of these runs contained a ghost particle with initial rotation axis identical to the standard Earthmoos. Fig. 5 shows the difference in obliquity between two runs with differing initial Mars positions as a function of time, and Fig. 3 and the range bars near 0° in Fig. 6 show the net short-term (defined as ± 1 Myr), medium-term (± 500 Myr) and long-term (full integration) obliquity ranges for Earthlike initial axis orientation in the orbital chaos runs. The Mars-ahead run shows typical orbital variations out to 800 Myr into the future, but then Mercury's eccentricity grows and it jumps up to 0.7 at +900 Myr. This type of Solar System instability has been seen before, and is described elsewhere (Laskar and Gastineau, 2009, and references therein). It yields a Solar System different from the present state (which was used for the frequency map analysis of Laskar et al. (1993b)), so we truncate this run at 800 Myr for the obliquity studies presented herein.

From Fig. 5, we calculate that the Lyapunov time for orbital chaos is 7 Myr. Hence when orbital chaos is present, the chaotic evolution of Earthmoos obliquities is driven by chaotic orbits more than by inherent chaos in the obliquity itself.

As expected based on the Lyapunov time, the short-term obliquity range is identical for the same initial conditions in the nominal, ahead, and behind systems. Over the full time of the integration, however, chaos drives the ranges to differ, sometimes by a few degrees, but occasionally by more. The substantial regime shifts shown in Fig. 2 do not occur in the majority of other integrations.

5. Axis orientation

In addition to the chaotic variability of past and future obliquity, the obliquity evolution of Earthmoos depends strongly on our broadly-chosen initial conditions. In Sections 3 and 4, we chose an initial obliquity $\Psi \approx 23.44^\circ$, the same as Earth's real obliquity today. We might alternatively have chosen a different obliquity

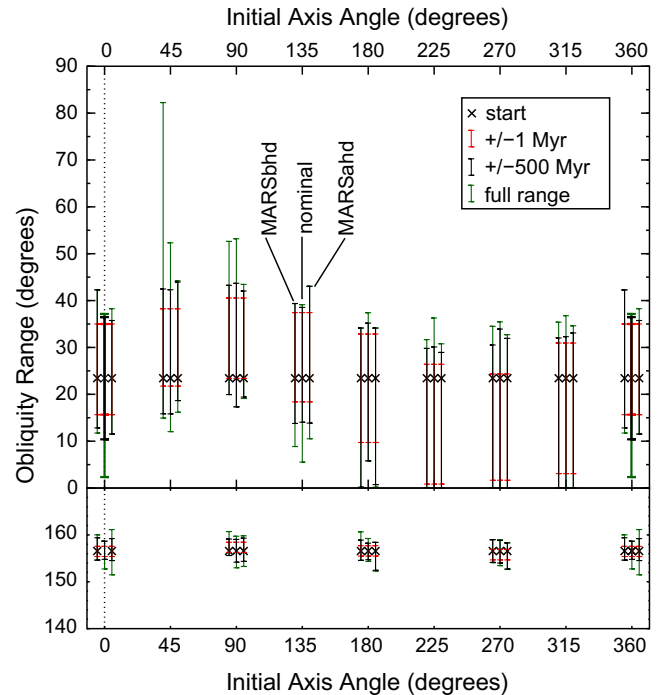


Fig. 6. Aggregated results from three different runs to show orbital chaos that used differing initial rotation axis azimuths. All of the planets have the same initial obliquity of 23.44° in the top box, and retrograde obliquity of 156.56° in the bottom box. The bold range corresponds to the ‘standard’ Earthmoos. The middle range of each threesome corresponds to integrations of a nominal Solar System. Those to the right and have Mars moved 1 m ahead in its orbit and behind in its orbit, respectively; they have the same axis angle as the nominal run, but are offset horizontally for clarity. These are effectively different possible obliquity evolutions allowed, and equally valid, in the chaotic regime. The red bars show the obliquity sampled during the interval (± 1 Myr). Black bars show the extension of the range of obliquity during the interval (± 500 Myr). Green bars show the obliquity range over the entirety of the relevant integration. The ‘full’ range is -2 to $+1.18$ Gyr for the middle (nominal) integration, -1.73 to $+0.8$ Gyr for the right (MARSahd) integration, and -2.0 to $+1.12$ Gyr for the left (MARSbhd) integration. The MARSahd integration was truncated at $+0.8$ Gyr due to atypical orbit behavior. (For interpretation of the references to color in this figure legend, the reader is referred to the web version of this article.)

between 22.1° and 24.5° , the range over which Earth's obliquity varies due to the Milankovitch cycles.

We might also have elected to have the same value for Earth's obliquity, but to have the Earth's axis pointed in a different direction. To put this another way, we could use the same obliquity for the Earth, but change the date of the northern spring equinox. We call this angle the axis azimuth, φ . We define $\varphi = 0^\circ$ to be Earth's present-day axis azimuth, and positive values of φ such that they correspond to later times for the northern spring equinox. We integrated seven such ghost planets, spaced by 45° in φ ; the results are shown in Fig. 6. As evident from the comparison of displayed ranges, the obliquities of these planets differ from that of the nominal Earthmoos by more than the effects of chaos, especially on sub-Gyr timescales.

Fig. 7 shows ± 2 Gyr obliquity evolution for Earthmoos with initial axis angles $\varphi_0 = 0^\circ, 90^\circ, 180^\circ,$ and 270° . They correspond to having the northern spring equinox at the present epoch on \sim March 21, June 21, September 21, and December 21 respectively. While all of these integrations have identical obliquities, $\Psi = 23.44^\circ$, the character of their evolutions differ significantly. The integration with $\varphi_0 = 180^\circ$, third panel down in Fig. 7, has strong qualitative similarity to the $\varphi_0 = 0^\circ$ case reproduced at top for comparison (these data are the same as those in Fig. 2). It varies rapidly between an obliquity of $\Psi \sim 10^\circ$ and $\Psi \sim 40^\circ$, but stays

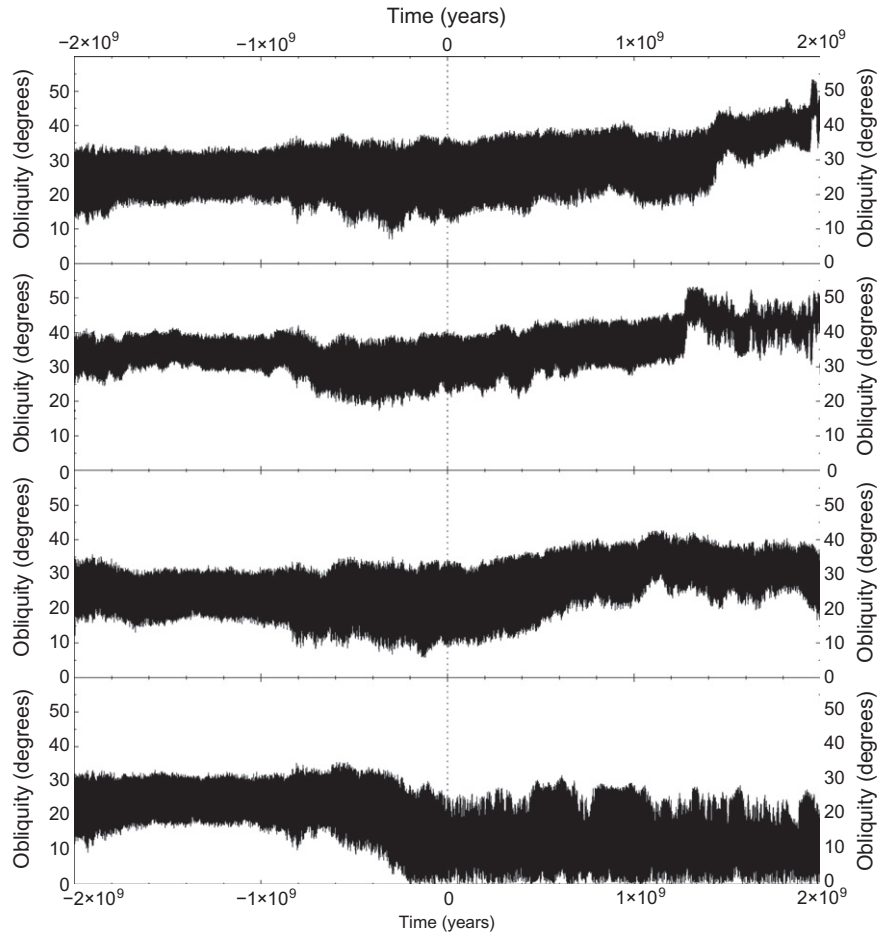


Fig. 7. Long-term obliquity evolution for Earthmoons with the same initial obliquity as Earth, but differing initial azimuthal axis orientations, φ_0 , that are 0° (top), 90° (second from top), 180° (third from top), and 270° (bottom) ahead of the present-day axis orientation.

constrained between those obliquity values over the entire 4 Gyr integration. Second from the top in Fig. 7, the $\varphi_0 = 90^\circ$ integration constrains obliquity to between $\Psi \sim 20^\circ$ and $\Psi \sim 40^\circ$ until 1.3 Gyr hence. At 1.3 Gyr the obliquity evolution changes regime, and thereafter is bracketed by $\Psi \sim 30^\circ$ and $\Psi \sim 50^\circ$. Fig. 7's bottom figure, for $\varphi_0 = 270^\circ$, shows the opposite change. This integration has obliquity evolution between $\Psi \sim 10^\circ$ and $\Psi \sim 35^\circ$ in the distant past, but then has obliquities dropping to $0^\circ < \Psi < 30^\circ$ from 200 Myr ago until the end of the integration at 2 Gyr in the future.

The drops to low obliquity seen in the latter case have the most serious implications for climatic stability. Fig. 1 shows the year-averaged insolation as a function of latitude for planets with varying obliquities. Although high-obliquity planets have extreme seasons, the total solar heating is such that all latitudes receive a substantial flux over the course of the year. The greatest insolation disparity occurs with $\Psi = 0^\circ$. In that case, formally the poles receive no solar flux at all (we have neglected atmospheric scattering). Barring a massive atmospheric or oceanic heat transport, there exists the likelihood that the poles of an Earth-like planet would then freeze over. If the resulting glaciation is severe enough it could enter into a runaway snowball state (Hoffman et al., 1998) that would be detrimental to any multicellular life on the planet.

Each of these integrations with varying initial axis azimuth φ are roughly equally valid. Given the present rapid rotation axis precession resulting from lunar torques, the real Earth's φ proceeds from 0° around to 360° every 26 kyr. Since the Earth's rotation axis precesses in the opposite direction from Earth's orbital

motion, the $\varphi = 90^\circ$ case roughly corresponds to an Earthmoon integration with initial rotation axis pointed as it was 6500 years ago. The $\varphi = 270^\circ$ case represents the obliquity evolution that would occur if we started the rotation axis in the orientation that it will be 6500 years from now. These differences result from variations in Earth's orbital plane. Since obliquity is defined as the angle between a planet's rotational axis and the normal to its orbit, both changes in the absolute position of the orbital axis and changes in the orbital pole both affect obliquity. Earth's orbital plane precesses around the Solar System's invariable plane (perpendicular to the net Solar System angular momentum vector) with a period of ~ 100 kyr. The rotational axis of an Earthmoon has a precession period comparable to that of Earth's orbit plane. This near-resonance drives the large short-term variability of Earthmoon obliquity.

6. Initial obliquity

Terrestrial planet formation is chaotic. Without a giant Moon-forming impact, or with a different one, the initial obliquity of an Earthmoon would typically differ from that of the present-day Earth. Neron de Surgy and Laskar (1997) show that billions of years ago the real Earth's obliquity was substantially different than it is in the present epoch. Using the Earth's present obliquity of 23.44° as the starting condition for calculating the obliquity evolution of an Earthmoon does not tell the whole story. We thus ran numerous

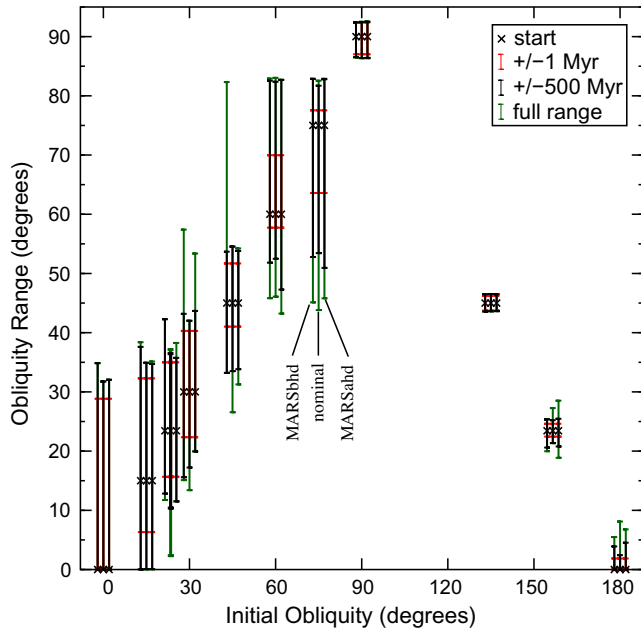


Fig. 8. Aggregated results from each of our runs to show orbital chaos for differing initial Earthmoo obliquities. The middle range of each group corresponds to integrations of a nominal Solar System. Those to the right and have Mars moved 1 m ahead in its orbit and behind in its orbit, respectively. These are effectively different possible obliquity evolutions allowed, and equally valid, in the chaotic regime. The red bars show the obliquity sampled during the interval (± 1 Myr). Black bars show the extension of the range of obliquity during the interval (± 500 Myr). Green bars show the obliquity range over the entirety of the relevant integration. The ‘full’ range is -2 to $+1.18$ Gyr for the middle (nominal) integration, -1.73 to $+0.8$ Gyr for the right (MARSahd) integration, and -2.0 to $+1.12$ Gyr for the left (MARSbhd) integration. The MARSahd integration was truncated at $+0.8$ Gyr due to atypical orbit behavior. (For interpretation of the references to color in this figure legend, the reader is referred to the web version of this article.)

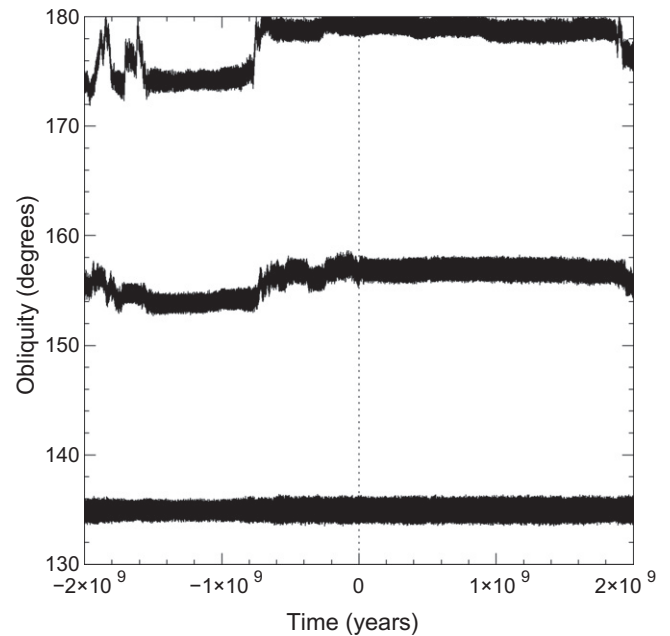


Fig. 10. Gyr-scale obliquity evolution of retrograde Earthmoos with initial obliquities of 180° (top curve), 156.5° (middle curve), and 135° (bottom curve). Though the retrograde rotators have smaller variability than do prograde Earthmoos, their Gyr-scale behavior is analogous in that they experience long periods of obliquity constrained within a narrow band punctuated by short transitions to different obliquity regimes.

ghost particles with initial obliquities substantially different from the Earth’s present obliquities in the integrations with Mars ahead of or behind its nominal position by 1 m. The results of these simulations are presented in Fig. 8.

6.1. Prograde

We plot the obliquity evolution for hypothetical Earthmoos with different prograde obliquities in Fig. 9. The integration that starts with obliquity $\Psi_0 = 0^\circ$ undergoes the same $\sim 100,000$ year short-term variations as the $\Psi_0 = 23.44^\circ$ Earthmoos. It also does not show large long-term excursions, however, and remains bounded between $\Psi = 0^\circ$ and $\Psi = 30^\circ$ throughout the ± 2 Gyr integration. Its overall behavior resembles that of the future of the $\Psi_0 = 23.44^\circ$ Earthmoo with initial axis azimuth $\varphi_0 = 270^\circ$ that we discuss in Section 5.

The Earthmoo with $\Psi_0 = 45^\circ$ shows the smallest variability of any of the prograde moonless Earths that we study. Its short-term obliquity varies in just a 10° range. On longer (10 Myr) timescales, that range shifts from as low as $30\text{--}40^\circ$ up to $40\text{--}50^\circ$.

At higher obliquity, the $\Psi_0 = 75^\circ$ Earthmoo shows a qualitatively different behavior. Its short-term obliquity variations sometimes occur over a 10° range, and sometimes over a 25° range from 55° to 80° . By 2 Gyr in the future this Earthmoo has undergone a regime shift such that its obliquity is confined between 45° and 55° ; its envelope overlaps that of the $\Psi_0 = 45^\circ$ Earthmoo on the plot.

Of these three prograde integrations, with $\Psi_0 = 0^\circ$, 45° , and 75° , the low obliquity may be the most dangerous for climatic stability. As shown in Fig. 1, the yearly averaged solar flux between an obliquity of 0° and 20° differs more than that between 40° and 60° . In the end, however, a more sophisticated treatment would be necessary in order to assess the habitability of worlds with the type of obliquity variations that we find.

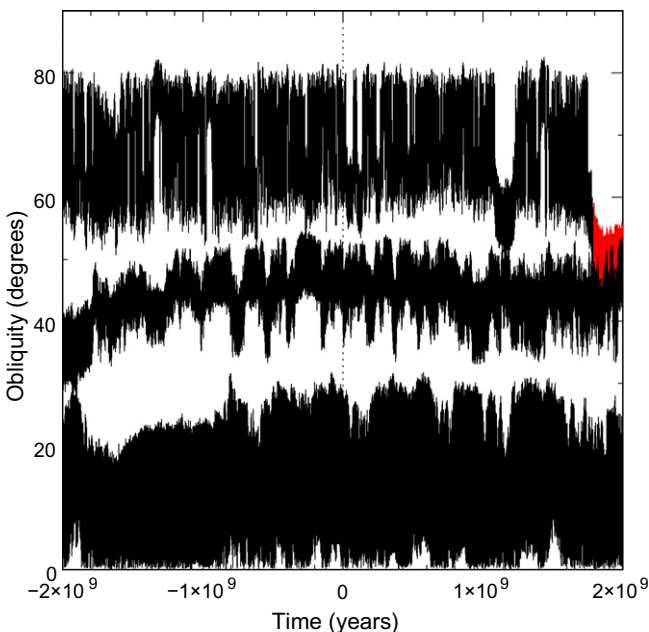


Fig. 9. Gyr-scale obliquity evolution of prograde Earthmoos with initial obliquities of $\Psi_0 = 75^\circ$ (top curve), $\Psi_0 = 45^\circ$ (middle curve), and $\Psi_0 = 0^\circ$ (bottom curve). The $\Psi_0 = 75^\circ$ curve is in red (and behind) where it overlaps the $\Psi_0 = 45^\circ$ curve for clarity. (For interpretation of the references to color in this figure legend, the reader is referred to the web version of this article.)

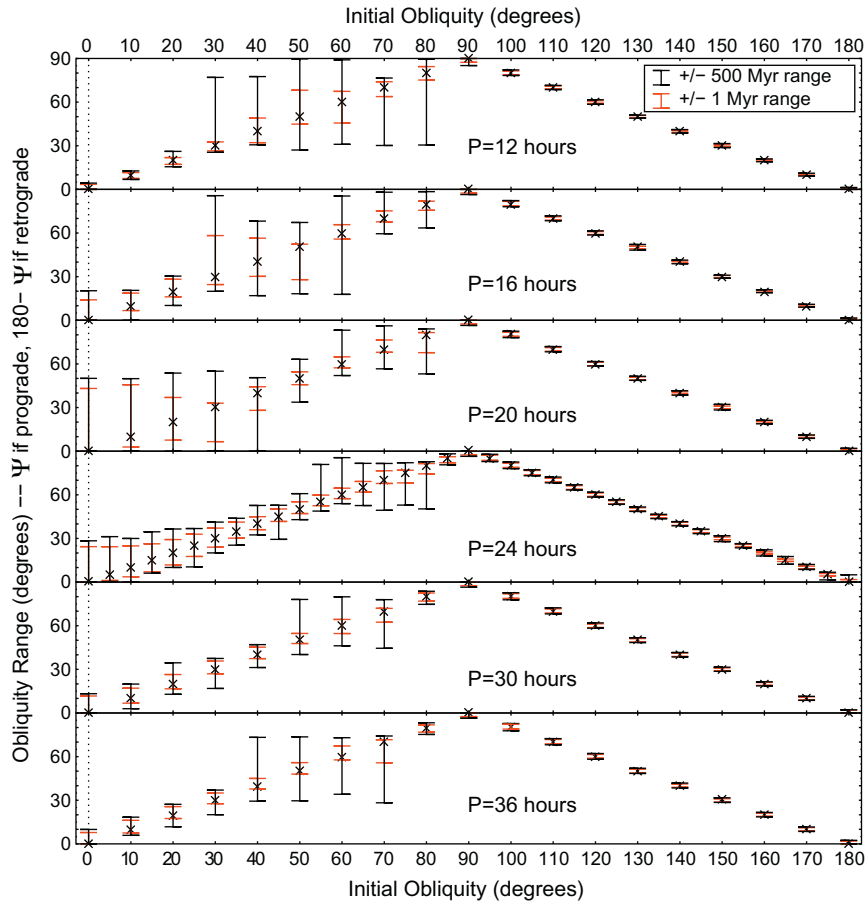


Fig. 11. Range of obliquity variations for Earthmoons with varying rotation periods P . The initial obliquity is given on the horizontal axis (from 0° to 180°) and by the black \times on the range bar. Obliquity ranges are shown on the vertical axis, with retrograde values shown as $180^\circ - \Psi$. The red bars show the obliquity sampled during the interval (± 1 Myr). Black bars show the extension of the range of obliquity during the interval (± 500 Myr). These particular integrations were discontinued at ± 500 Myr, so no green bars analogous to those in Figs. 3, 6, 8, 12 and 13 are needed. (For interpretation of the references to color in this figure legend, the reader is referred to the web version of this article.)

6.2. Retrograde

Planets that rotate retrograde (*i.e.*, $\Psi > 90^\circ$) experience rotational axis precession in the opposite sense as those that rotate prograde. Hence while prograde rotators can have their rotational precession enter into resonance with orbital precession, under most circumstances retrograde rotators cannot. Thus retrograde-rotating planets would be expected to have more stable obliquities than prograde rotators.

Our analysis agrees with past studies (*e.g.*, Laskar et al., 1993b) that they are. Fig. 10 shows the obliquity evolution for retrograde planets with $\varphi_0 = 135^\circ$, $\varphi_0 = 155^\circ$, and $\varphi_0 = 180^\circ$. The short-period obliquity variations for the $\varphi_0 = 135^\circ$ and $\varphi_0 = 155^\circ$ retrograde Earthmoons are constrained over a range of just 2° – less than the obliquity variability of the real Earth. Therefore the climatic variations on these planets should also be similar to that of the real Earth. If the initial axis orientations of terrestrial planets are isotropic (Miguel and Brunini, 2010), then half should be retrograde. Severe obliquity-driven climatic shifts will not affect those half, and not inhibit their habitability.

7. Rotation rate

To this point we have considered Earthmoons with the same rotation rate as the present Earth. While this choice is a reasonable

starting point, the initial rotation period of a moonless Earth might be anything from the theoretical minimum of ~ 2.8 h to weeks or longer. We therefore ran a set of integrations for hypothetical Earthmoons with rotation periods between 2.8 h and 48 h at varying initial obliquities and axis angles in order to explore their obliquity evolution. The long-term obliquity variations for these faster- and slower-spinning Earthmoons are shown in Figs. 11–13.

Earthmoons with rotation rates leading to axis precession rates nearly commensurate with orbital precession are expected to have the most variable obliquities. The obliquity for Earthmoons with rotation rates far from this commensurability can be quite stable. Most of the Earthmoons with very rapid rotations, those with periods of 2.8 h and 4 h, show total obliquity variability of $\sim 1^\circ$ – less than that of the real (mooned) Earth. The 4-h period Earthmoon with initial obliquity of 90° has a wider obliquity variation range, between 70° and 93° , but that range is consistent over Gyr timescales.

With increasing rotation periods around 12 h the obliquity range increases, but the variations remain somewhat stable over long timescales. The obliquity evolution for these rotation rates is chaotic for some initial obliquities (23.44° and 45° from Fig. 8), and not for the rest.

At longer rotation periods, the obliquity of Earthmoons with initial obliquity of 90° remains near this value. The obliquities of Earthmoons with initial obliquity between 0° and 45° all vary substantially for the rotations periods that we study longer than 12 h. However, typical ranges are ~ 10 – 20° in width on megayear

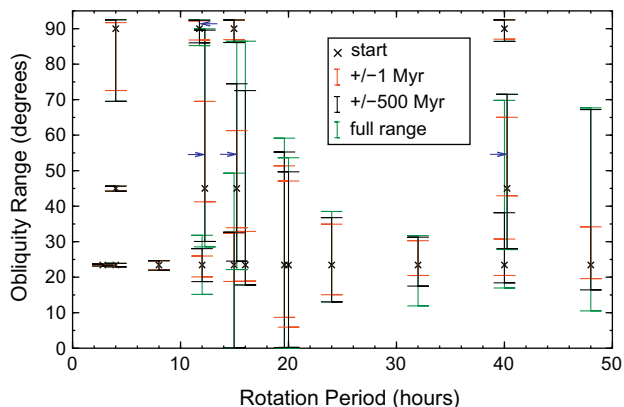


Fig. 12. This figure summarizes the obliquity range results for Earthmoons of varying initial rotation period. All planets have a calculated J_2 from the Darwin–Radau approximation (see Section 2.2). Rotation period 2.8 corresponds to a theoretical minimum rotation period for Earth. Other values not at multiples of 4 h are 14.9590278 h and 19.6183971 h, for comparison with Laskar and Robutel (1993). The red bars show the obliquity sampled during the interval (± 1 Myr). Black bars show the extension of the range of obliquity during the interval (± 500 Myr). Green bars show the obliquity range over the entirety of the relevant integration: ± 1.6 Gyr for those starting with $\Psi = 23.44^\circ$, and ± 1.15 Gyr for other starting obliquities. Range bars with blue arrows are offset from their actual rotation period in the direction indicated in order to maximize clarity by minimizing overlaps with other range bars. (For interpretation of the references to color in this figure legend, the reader is referred to the web version of this article.)

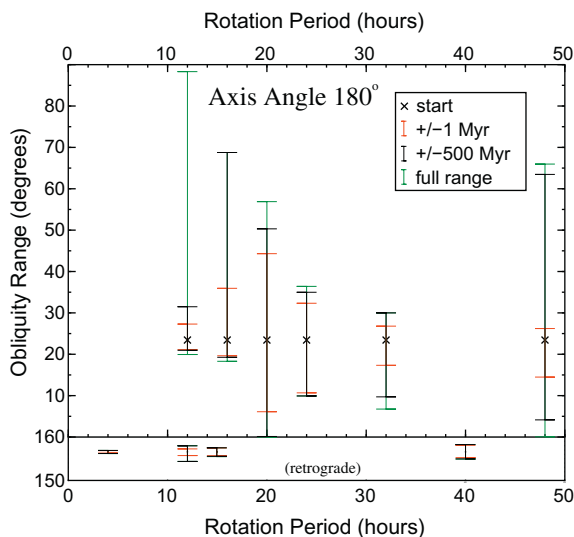


Fig. 13. Obliquity ranges for a select set of prograde and retrograde Earthmoons with obliquities of $\Psi = 23.44^\circ$ and $\Psi = 156.56^\circ$ but axis azimuths of $\phi = 180^\circ$, i.e., the dates of southern and northern spring equinox are reversed at $t = 0$ relative to those of the actual Earth at the present epoch. The red bars show the obliquity sampled during the interval (± 1 Myr). Black bars show the extension of the range of obliquity during the interval (± 500 Myr). Green bars show the obliquity range over the entirety of the relevant integration: ± 1.6 Gyr for the prograde planets in the upper panel, and ± 1.15 Gyr for the retrograde planets in the lower panel. (For interpretation of the references to color in this figure legend, the reader is referred to the web version of this article.)

timescales and ~ 20 – 30° wide on gigayear timescales, implying that climatic variations may be less severe than previously thought.

8. Conclusion

A frequency-map analysis by Laskar and Robutel (1993) concluded that a moonless Earth’s obliquity could vary anywhere between 0° and 85° . To investigate whether moonless Earths really

do access those different obliquities, we developed a module for the orbital integrator *mercury* to calculate and record the orientation of a planet’s rotational axis over time. As *mercury*’s calculation of planetary orbits dominates the computation time, we implemented a scheme whereby many “ghost planets” with positions fixed to that of the moonless Earth could all have their obliquity tracked simultaneously. This allows us to study different initial conditions for planetary obliquity and axis azimuth more efficiently.

Over the course of a 4 Gyr integration from 2 Gyr in the past to 2 Gyr in the future, we found that the obliquity of a moonless Earth is likely to remain within limits much more constricted than the range allowed by frequency-map analysis. Using Earth’s present day obliquity and axis orientation as the initial conditions, over 4 Gyr the obliquity varies between $\sim 10^\circ$ and $\sim 50^\circ$. This same integration shows long quiescent periods over 500 Myr in duration where the obliquity varies between 17° and 32° . These long quiescent periods are separated by intervals a few Myr long when the obliquity variation regime shifts to a different range.

None of our integrations show obliquity changes over the entire frequency-map allowed range. The behavior of obliquity depends strongly on the initial conditions. Small variations in those initial conditions result in chaotic changes in obliquity with a Lyapunov time of 7 Myr if initial orbits differ slightly, and 14 Myr for ghost particles with slightly different obliquities within the same orbital integration. Integrations of moonless Earths with initial obliquity the same as the real Earth’s, but with different rotational axis orientations, show similarly restricted obliquity variations that occur within different ranges.

Thus we assess that moonless Earths are probably able to access a good fraction of the range of obliquities allowed by frequency map analysis, but the typical timescale to explore this region may be longer than the typical lifetime of a solar-type star, or at least longer than the time that lapsed on Earth since the Cambrian diversification.

Hypothetical moonless Earths with differing prograde obliquities show qualitatively similar behavior. In those cases, obliquities vary over a $\sim 25^\circ$ range, within which lies the initial obliquity. Retrograde-rotating planets, whose rotational axis then precesses in the opposite sense as the orbital plane, show short-term obliquity variations of order just 2° , with infrequent regime-shifts of 4 – 5° . If initial planetary rotational axis orientations are isotropic, then half of all moonless extrasolar planets would be retrograde rotators, and these planets should experience obliquity stability similar to that of our own Earth, as stabilized by the presence of the Moon. Thus the presence of a large moon should not be considered a requirement for an earthlike planet to possess a stable enough obliquity for advanced life to develop and flourish.

Acknowledgments

The initial portions of this work were funded by NASA’s Exobiology program. Support for the completion of this study was provided by the NASA Origins of Solar Systems Program (J.E.C.) and by NASA’s Planetary Geology and Geophysics Program through RTOP 344-30-50-01 (J.J.L.). J.W.B. acknowledges the support of the NASA Postdoctoral Program, administered for NASA by Oak Ridge Associated Universities, and the NASA Exobiology program. The authors thank Tony Dobrovolskis and Elisa Quintana for careful reviews and useful manuscript comments.

Appendix A. Rotation rate and dynamical oblateness parameter determination

Simulations of the obliquity evolution of Earthmoons with a wide range of rotation rates are discussed in Section 7. Here we show

how we determined the initial parameters for Earthmoos with rotation rates differing from that of the real Earth. To analytically estimate what the J_2 and R_{eq} should be for each of our Earthmoos, we start with the Darwin–Radau relation, which relates J_2 and oblateness ($f \equiv (R_{eq} - R_p)/R_{eq}$ with R_p as the planet's polar radius – this is sometimes referred to as the dynamical ellipticity) as a function of C (Murray and Dermott, 2000):

$$\frac{J_2}{f} = -\frac{3}{10} + \frac{5}{2}C - \frac{15}{8}C^2. \quad (\text{A1})$$

Using the Darwin–Radau relation (Eq. (A1)) along with the relation that

$$f = \frac{3}{2}J_2 + \frac{1}{2}q, \quad (\text{A2})$$

where

$$q \equiv \frac{\Omega^2 R_{eq}^3}{GM_p}, \quad (\text{A3})$$

with G as the gravitational constant (Murray and Dermott, 2000), allows us to calculate that

$$J_2 = \frac{1}{3} \left(\frac{5q}{D} - q \right), \quad (\text{A4})$$

with D defined to be

$$D \equiv \frac{25}{4} \left(\frac{3}{2}C - 1 \right)^2 + 1. \quad (\text{A5})$$

With the definition of f , Eq. (A2) and conservation of the planet's volume such that

$$\frac{4\pi R_{eq}^2 R_p}{3} = \frac{M_p}{\rho} \quad (\text{A6})$$

(assuming that ρ remains constant as a function of Ω), it can be shown that

$$1 - \frac{3M_p}{4\pi R_{eq}^3 \rho} = \frac{3}{2}J_2 + \frac{1}{2}q. \quad (\text{A7})$$

Solving Eqs. (A4) and (A7) simultaneously by eliminating J_2 results in a multivalued quadratic expression for R_{eq} :

$$R_{eq}^3 = \frac{GM_p D}{\Omega^2} \left(2 \pm \sqrt{4 - \frac{30\Omega^2}{\pi\rho G D}} \right). \quad (\text{A8})$$

The double-valuedness results from there being two compatible angular momentum states for each given rotation rate. In the trivial case where $\Omega = 0$ the angular momentum states are that with zero angular momentum and zero oblateness, and that of infinite angular momentum as a flat pancake with $R_{eq} = \infty$. As the giant pancake

is unphysical, we keep only the negative root of the radical in Eq. (A8). We assign for our various Earthmoos a radius such that

$$R_{eq}^3 = \frac{GM_p D}{\Omega^2} \left(\frac{2 - \sqrt{4 - \frac{30\Omega^2}{\pi\rho G D}}}{10} \right), \quad (\text{A9})$$

and a J_2 from using a defined rotation rate with Eq. (A9) to determine q , which we plug back into Eq. (A4). When applied to the real Earth, the resulting system approximates Earth's equatorial radius to within 250 m and its J_2 to within 2%. To calculate the resulting oblateness f , plug the resulting J_2 back into Eq. (A2).

References

- Ahrens, T., 1995. Global Earth Physics. American Geophysical Union.
- Chambers, J.E., 1999. A hybrid symplectic integrator that permits close encounters between massive bodies. *Mon. Not. R. Astron. Soc.* 304, 793–799.
- Danby, J.M.A., 1988. *Fundamentals of Celestial Mechanics*, second ed. Willmann-Bell, Richmond, VA, USA.
- Dobrovolskis, A.R., 2009. Insolation patterns on synchronous exoplanets with obliquity. *Icarus* 204, 1–10.
- Goldsmith, J., Owen, T., 2002. *The Search for Life in the Universe*, third ed. University Science Books, Sausalito, California, USA.
- Hoffman, P.F., Kaufman, A.J., Halverson, G.P., Schrag, D.P., 1998. A neoproterozoic snowball Earth. *Science* 281, 1342–1346.
- Laskar, J., 1989. A numerical experiment on the chaotic behaviour of the Solar System. *Nature* 338, 237–238.
- Laskar, J., Gastineau, M., 2009. Existence of collisional trajectories of Mercury, Mars and Venus with the Earth. *Nature* 459, 817–819.
- Laskar, J., Robutel, P., 1993. The chaotic obliquity of the planets. *Nature* 361, 608–612.
- Laskar, J., Joutel, F., Boudin, F., 1993a. Orbital, precessional, and insolation quantities for the Earth from –20 Myr to +10 Myr. *Astron. Astrophys.* 270, 522–533.
- Laskar, J., Joutel, F., Robutel, P., 1993b. Stabilization of the Earth's obliquity by the Moon. *Nature* 361, 615–617.
- Laskar, J., Correia, A.C.M., Gastineau, M., Joutel, F., Levrard, B., Robutel, P., 2004. Long term evolution and chaotic diffusion of the insolation quantities of Mars. *Icarus* 170, 343–364.
- Lissauer, J.J., Berman, A.F., Greenzweig, Y., Kary, D.M., 1997. Accretion of mass and spin angular momentum by a planet on an eccentric orbit. *Icarus* 127, 65–92.
- Lissauer, J.J., Dones, L., Ohtsuki, K., 2000. Origin and evolution of terrestrial planet rotation. In: Canup, R.M., Righter, K. (Eds.), *Origin of the Earth and Moon*. University of Arizona Press, Tucson, pp. 101–112.
- Lunine, J., 2005. *Astrobiology: A Multidisciplinary Approach*. Pearson Addison-Wesley, San Francisco, California, USA.
- Miguel, Y., Brunini, A., 2010. Planet formation: Statistics of spin rates and obliquities of extrasolar planets. *Mon. Not. R. Astron. Soc.* 406, 1935–1943.
- Murray, C.D., Dermott, S.F., 2000. *Solar System Dynamics*. Cambridge University Press, New York.
- Neron de Surgy, O., Laskar, J., 1997. On the long term evolution of the spin of the Earth. *Astron. Astrophys.* 318, 975–989.
- Schlichting, H.E., Sari, R., 2007. The effect of semicollisional accretion on planetary spins. *Astrophys. J.* 658, 593–597.
- Touma, J., Wisdom, J., 1994. Lie–Poisson integrators for rigid body dynamics in the Solar System. *Astron. J.* 107, 1189–1202.
- Ward, P., Brownlee, D., 2000. *Rare Earth: Why Complex Life is Uncommon in the Universe*. Copernicus, New York.
- Wisdom, J., Holman, M., 1991. Symplectic maps for the N-body problem. *Astron. J.* 102, 1528–1538.